Processing and Application of Ceramics 12 [4] (2018) 394–402
https://doi.org/10.2298/PAC1804394L



# Dielectric, ferroelectric and magnetic properties of $Bi_{0.78}La_{0.08}Sm_{0.14}Fe_{0.85}Ti_{0.15}O_3$ ceramics prepared at different sintering conditions

Zhengxin Li[1,2], Zhenhua Wang[1,2], Rongli Gao[1,2,*], Wei Cai[1,2], Gang Chen[1,2], Xiaoling Deng[1,2], Chunlin Fu[1,2,*]

[1]*School of Metallurgy and Materials Engineering, Chongqing University of Science and Technology, Chongqing 401331, China*
[2]*Chongqing Key Laboratory of Nano/Micro Composite Materials and Devices, Chongqing 401331, China*

Received 25 June 2018; Received in revised form 23 October 2018; Accepted 12 December 2018

## Abstract

*Although $BiFeO_3$ (BFO) has attracted great attention due to its special physical properties as a typical single phase multiferroic material, the application is limited due to the formation of impurities, defects and so forth. Herein, we report improved multiferroic properties of $Bi_{0.78}La_{0.08}Sm_{0.14}Fe_{0.85}Ti_{0.15}O_3$ (BLSFTO) ceramics by combination of co-doping and sintering schedule. BLSFTO multiferroic ceramics were prepared by using the conventional solid state reaction method and the effect of sintering time (2, 5, 10, 20 and 30 h) on the structural, dielectric and multiferroic properties was investigated systematically. The result indicates that stable BLSFTO phase with perovskite structure was formed for all the samples. Only some impurities such as $Bi_2O_4$ can be observed when the sintering time is longer than 20 h, indicating that the sintering time can induce structural changes in BLSFTO and too long sintering time can remarkably increase the secondary phases. In addition, the frequency dependent dielectric properties show that sintering time has distinct effect on the frequency stability and the relaxation process. The result demonstrates that the enhanced magnetization, improved dielectric and ferroelectric properties may be correlated with the structural transformation, impurities, oxygen vacancies and grain morphology.*

***Keywords:*** *$BiFeO_3$ ceramics, doping, sintering schedule, dielectric properties, multiferroic properties*

## I. Introduction

Multiferroic materials are a new kind of functional materials which simultaneously show magnetic and ferroelectric properties, but more importantly, these features can couple with each other, i.e. the magnetic properties can be tuned by external electric field and vice versa [1–3]. Based on these special characteristics, multiferroic materials have gained extensive attention for several decades owing to their interesting physical properties and potential applications in sensors, storages, capacitors, spintronic devices etc. [4–6]. Among them, $BiFeO_3$ (BFO) is one of the most widely studied multiferroic materials, which is considered as a perspective candidate for demanding applications in non-volatile memories, solar cells and multi-functional sensors because of its high remnant polarization (~100 mC/cm$^2$), relatively small band gap (~2.7 eV), large absorption coefficient ($10^4 \sim 10^5$ cm$^{-1}$ at 400 nm), multi-domain structure as well as its multiferroic properties above room temperature [7,8]. However, in the rhombohedral *R3c* phase of BFO, the macroscopic magnetization cancels due to the G-type antiferromagnetic (AFM) spin configuration, inhibiting their use in practical applications [9–11]. Moreover, from a practical application perspective, in addition to its weak magnetization, several drawbacks need to be addressed for BFO. One serious problem is the high leakage current density which mainly results from the existence of impurities, such as $Bi_2Fe_4O_9$, the valence change of ions $Fe^{3+} \rightarrow Fe^{2+}$, and defects such as oxygen vacancies. In BFO, these draw-

*Corresponding authors: tel: +86 23 65023707,
e-mail: *gaorongli2008@163.com* (Rongli Gao)
*chlfu@126.com* (Chunlin Fu)

backs naturally result in inferior ferroelectric, dielectric and magnetic properties [12–14]. On the other hand, the volatilization of Bi element at high temperature and the low thermal stability of BFO provide an obstacle to the conventional ceramics processing of this material because of the narrow processing window. As a consequence, the formation of impurity phases always provides an additional difficulty in the physical characterization. Hence, to improve the multiferroic properties, it is essential to develop effective synthesis strategies to obtain BFO sample without any secondary or impurity phases, because these unwanted phases always seriously screen the potential properties of BFO.

In order to overcome these shortcomings mentioned above and considering the fact that part of the problems lie in the volatility of bismuth, site engineering (doping at the A site or B site or both of A and B sites) concept has been widely explored to reduce the leakage current and enhance its magnetic and electric properties. From the viewpoint of general theories and experiments, superior ferroelectric properties can be obtained through reduction of leakage current due to the suppression of oxygen vacancies with single doping or co-doping in BFO. Among these doped elements, Sm, La, Ca, Sr, Sc, V, Ni, Gd, Mn, Ti and Co, partially substituted at the A site or B site or both of A and B sites, have been reported to suppress the cycloid structure and therefore enhance homogenization of spin arrangement, improve the ferroelectric behaviour, and intensify the magneto-electric coupling in BFO [15–18].

Until now, many previous attempts have been made to investigate single doping or co-doped systems [19–22], and indeed, the multiferroic properties have been improved to some extent. Nevertheless, in such attempts either the percentage of substitution was low or only up to two elements were chosen to replace Fe or/and Bi element. On the other hand, there were few systematic studies of how the co-doped elements effect the microstructure, dielectric, magnetic and ferroelectric measurements. And more importantly, the best process parameters may be different for different doping elements or different doping content. Therefore, the optimal value for various performance aspects cannot be obtained with the same technology parameters. Particularly, the reason why technology parameters of synthesis method can control the physical properties of BFO is that the parameters play significant role in tuning the particle size and morphology. Among them, the sintering time is a dominant factor to decide the general performance of BFO samples. Accordingly, it is of great importance to investigate how sintering time affect the microstructure, dielectric, ferroelectric and magnetic properties of multiple doped BFO.

In this paper, we report the improved multiferroic properties of La, Sm and Ti co-doped BFO ceramics by appropriate sintering schedule, where La doping at the A site can reduce the leakage current, Sm doping at the A site can enhance ferroelectric properties, and Ti doping at the B site can improve magnetic properties [23–28]. The phase and morphology evolution of BFO with respect to the different sintering time as well as their influence on the physical properties such as electrical and magnetic properties of BFO have also been systematically discussed.

## II. Experimental procedure

$Bi_{0.78}La_{0.08}Sm_{0.14}Fe_{0.85}Ti_{0.15}O_3$ (BLSFTO) ceramics was prepared by conventional solid state reaction method. $Bi_2O_3$, $La_2O_3$, $Fe_2O_3$, $Sm_2O_3$ and $TiO_2$ were used as raw materials in terms of Bi : La : Sm : Fe : Ti = 0.86 : 0.08 : 0.14 : 0.85 : 0.15. Here, 8 at.% excessive Bi was used to compensate for the high volatilization of Bi during the sintering process. According to the atomic ratio, the raw materials were placed in a ball mill and mixed and thoroughly ground for 12 h. The ground powder was placed in a crucible and a box furnace for sintering at 700 °C for 2 h. After that, the sample powder was taken out and ground for 12 h in a ball mill and placed in a box oven for 2 h at 800 °C. Then, appropriate amount of organic binder polyvinyl alcohol (PVA) was added. Subsequently, the mixture was fully ground and pressed into a disk with a diameter of 10 mm and the thickness of about 0.8 mm. After that, the ceramic pellets were placed in a tube furnace and heated to 150 °C at a rate of 1 °C/min and then to 350 °C at a rate of 5 °C/min. Eventually, the ceramics was heated to 500 °C at a rate of 1 °C/min and maintained at 500 °C for 50 h so as to fully decompose and discharge the organic binder avoiding very rapid burning because pores in the ceramics are easy to form. Finally, the treated samples were then heated to 940 °C at a rate of 5 °C/min in a box oven and then maintained for 2, 5, 10, 20 and 30 h.

The crystal structure of all samples was examined at room temperature via X-ray diffraction (XRD, DX2700, China) with Cu K$\alpha$ radiation ($\lambda$ = 1.5406 Å). The surface morphology of the prepared ceramics was investigated by using scanning electronic microscopy (SEM, S3700, Hitachi, Japan) and EDS analysis mode was used to analyse compositional variations. In order to observe the grain structure and porosity more clearly, all the prepared specimens were polished and then thermally etched. To measure the electric properties, both surfaces of all the ceramics were polished and silver paste was painted on both sides as the electrodes. They are fired at 500 °C for 30 min to obtain good contact. The dielectric properties of the samples were determined by using a LCR instrument analyser (HP4980A, Agilent, USA). The dielectric constant was calculated from the capacitance using the following equation:

$$\varepsilon = \frac{C \cdot d}{\varepsilon_0 \cdot A} \tag{1}$$

where $C$ is the capacitance, $\varepsilon_0$ is the free space dielectric constant ($8.85 \times 10^{-12}$ F/m), $A$ is the effective area of the surface electrode and $d$ is the thickness of the

sample. The ferroelectric hysteresis loops (*P-E* curves) and conductive properties (*J-E* curves) were measured with the TF2000 ferroelectric test system (TF2000, aixACCT Inc., Germany). Magnetic properties were analysed by the vibrating sample magnetometer (VSM, ND105, China).

## III. Results and discussion

For comparison, the XRD patterns of all BLSFTO ceramics sintered for different periods are shown in Fig. 1a. One can find that all the diffraction peaks exhibit distorted hexagonal perovskite structure and are indexed with structure of BFO with *R*3*c* space group. The reaction kinetics of the formation of the BFO and the thermodynamic stability of BFO suggests the presence of some impurity peaks along with BFO when using the solid state reaction method [28–31]. It can be seen from Fig. 1 that the XRD patterns of the BLSFTO samples at different sintering time are consistent with the BFO pattern (JCPDS No. 74-2016). It should be pointed out that we cannot find proper BFO patterns that are fully con-

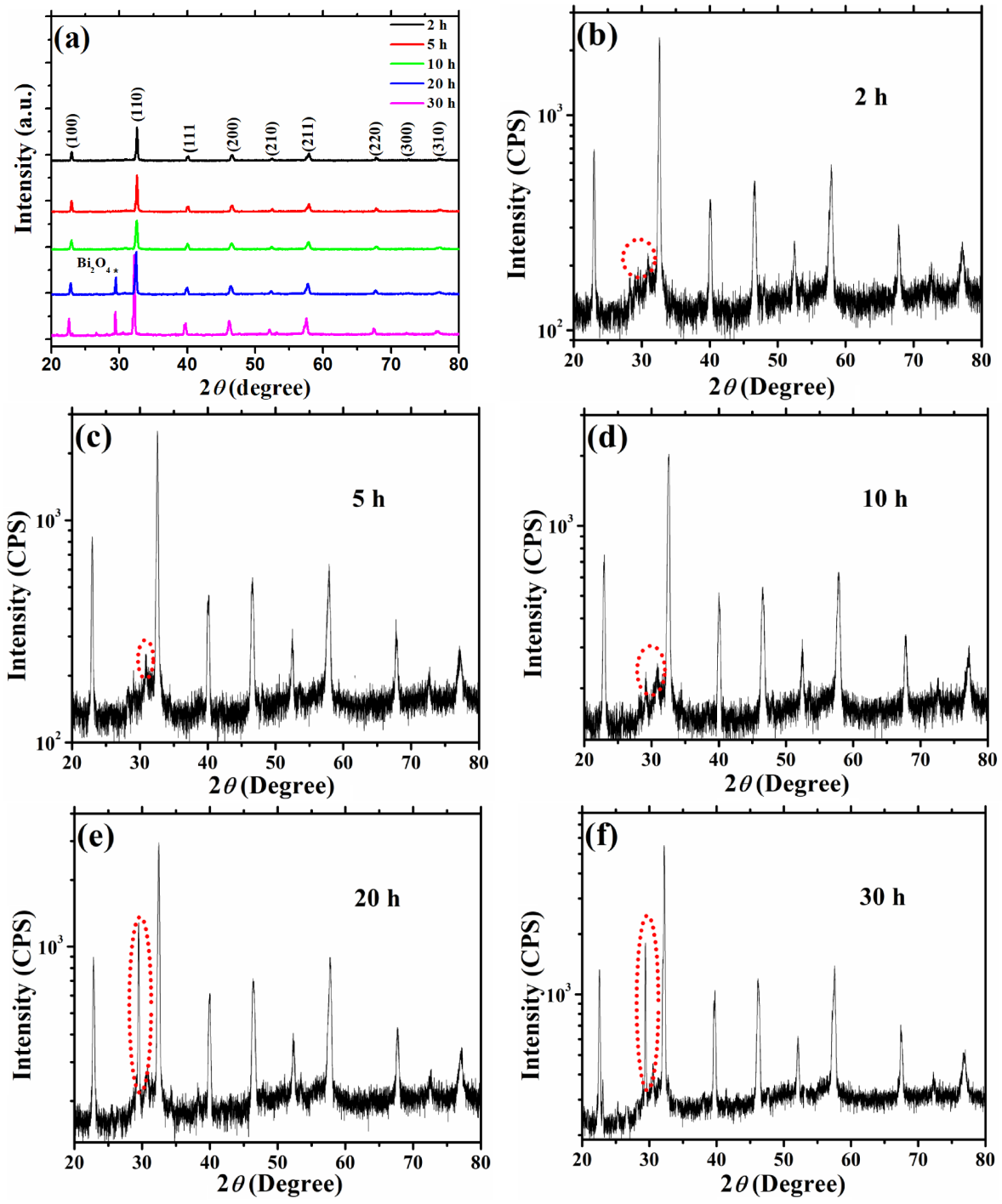


**Figure 1. XRD patterns of BLSFTO ceramics sintered for different period with linear coordinate (a) and semilogarithmic coordinates for: b) 2 h, c) 5 h, d) 10 h, e) 20 h and f) 30 h**

sistent with the XRD patterns of our samples. Overall, the patterns (JCSPDS No. 86-1518, 72-2035, 73-0548, 74-2016, etc.) are all similar to our XRD results, but all the XRD peaks of our samples are to some extent shifted to the right side of the standard XRD patterns. The reason for this phenomenon can be attributed to the doping and different sintering parameters. Finally, we have chosen the XRD pattern (JCSPDS No. 74-2016) as the standard card because of the relatively high similarity. It is very obvious that with the prolonging of the sintering time, the intensity of the diffraction peak of the sample gradually increases and becomes more and more sharp, indicating that the crystallization tends to be good. The corresponding hexagonal lattice parameters of the samples are listed in Table 1.

It should be noted that when the sintering time is less than 20 h, no other apparent secondary phases can be observed. However, when the sintering time is longer than 20 h, all the samples have small impurity peaks, which are marked by stars, as shown in Fig. 1a. When the sintering time is longer than 20 h, an additional diffraction peak from Bi oxide can be observed. This impurity phase is a consequence of the volatile Bi element because prolonged sintering time will result in more decomposition of BFO compounds. It can be seen that, when the sintering time is 10 h, the crystallization is good, without any miscellaneous peaks observed.

**Table 1. The lattice parameters of BLSFTO ceramics with different sintering time**

| Lattice parameter | Sintering time | | | | |
|---|---|---|---|---|---|
| | 2 h | 5 h | 10 h | 20 h | 30 h |
| *a* [Å] | 5.3699 | 5.5115 | 5.5117 | 6.5524 | 8.4782 |
| *c* [Å] | 14.3107 | 13.3158 | 13.3314 | 11.9412 | 10.3009 |

In order to show the possibility of the decomposition and formation of secondary phases for all the sintered samples, the XRD patterns were drawn in semi-logarithmic coordinates, as shown in Figs. 1b-1f. It is clear that in addition to the impurity phase $Bi_2O_3$, all samples show a low intensity peak when $2\theta = 26°$, and the secondary phase is indexed as $Bi_{3.43}Fe_{0.57}O_6$.

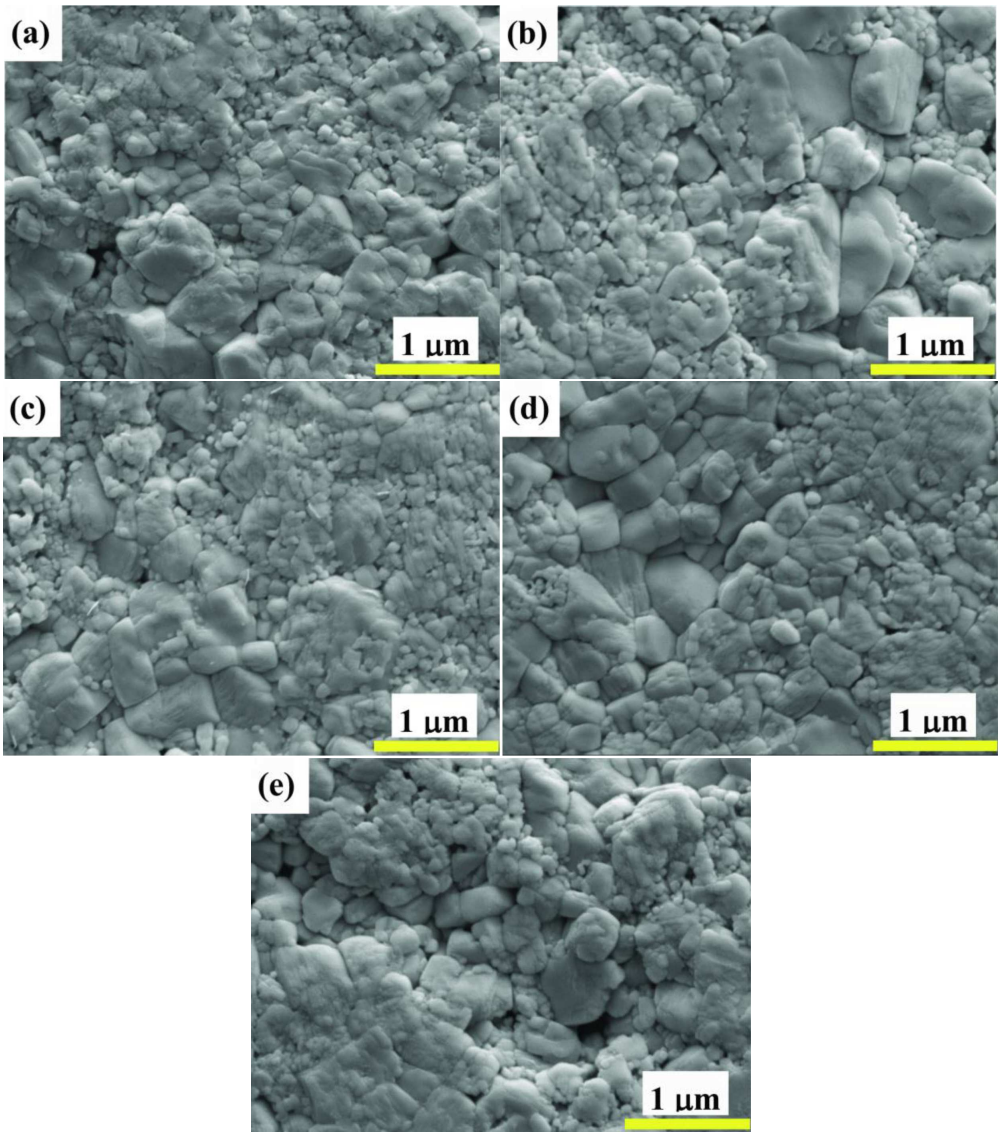


**Figure 2. SEM images of polished BLSFTO ceramics sintered at different times: a) 2 h, b) 5 h, c)10 h, d) 20 h and e) 30 h**

In addition, the peak intensity of the impurity increases with the increase of the sintering time, which is indexed with red circles in Fig. 1. This increased peak can be attributed to the decomposition of BFO based ceramics under long time and high temperature conditions.

In order to investigate the microstructure and surface morphology of the obtained BLSFTO ceramics sintered at different times, all the samples were polished and then thermally etched before SEM imaging, and the results are shown in Fig. 2. It is obvious that BLSFTO ceramics sintered with different times shows irregularly shaped grains and all the samples display relatively dense structure.

Clearly, pores of the BLSFTO samples gradually decrease with the increased sintering time, indicating that prolonging the sintering time can reduce the porosity of the ceramics and thus enhance the density, which can in turn result in the decrease of leakage current and theoretically enhance the ferroelectric properties. Moreover, with the extension of the sintering time, the grain size gradually becomes larger and non-uniform. The reason is that when the sintering time is shorter there will be less volatilization of Bi element and less defects such as oxygen vacancies will be generated. As a consequence, during the sintering process the movement of oxygen ions will slow down, which can reduce the growth rate of grains and result in the grain size being decreased. On the contrary, when the sintering time is too long, e.g. more than 20 h, it can lead to the evaporation of Bi element, which in turn results in the increase of oxygen vacancies, and the movement of oxygen ions will seems to speed up, therefore the grains continue growing.

To directly show the density of the prepared ceramics sintered for different time, Archimedes principle was employed. When the sintering time is 2, 5, 10, 20 and 30 h, the corresponding densities of the sample are 8.271, 8.267, 8.325, 8.371 and 8.450 g/cm$^3$, respectively. These measured densities are basically the same as the result 8.31 g/cm$^3$ concluded from the stand PDF card (JCSPDS No. 74-2016). This slight enhancement of density with the increase of sintering time can be ascribed to the increased compactness resulting from the large grains and less pores in the samples.

In order to analyse compositional variations of the samples with different sintering time, the EDS analysis mode was used and the results are shown in Fig. 3. Although the relative content of each element can vary, this is only perception because EDS images are not for the same sample and the content of oxygen is not precise since the oxygen is very light element. For the sake of analysis, all included elements in all samples were listed in Table 2 by considering the fact that the total sum of all elements should be 1 for both A and B site.

It can be seen from Table 2 that the relative content of Bi element decreases with the sintering time, indicating that Bi element under high temperature was volatilized and this volatilization increases with the time. Meanwhile, La and Sm elements show relative stability because no volatilization happened in the sintering process. In addition, Fe and Ti still maintain constant with different sintering time, as shown in Table 2. The relative contents of Fe and Ti element are about 85 and 15 at.%, respectively, roughly consistent with the calculated values in the nominal chemical formula, i.e., $Bi_{0.78}La_{0.08}Sm_{0.14}Fe_{0.85}Ti_{0.15}O_3$.

**Table 2. Relative element content of the samples sintered for different time**

| | Bi | La | Sm | Fe | Ti |
|---|---|---|---|---|---|
| Calculated value* | 0.78 | 0.08 | 0.14 | 0.85 | 0.15 |
| Measured value, 2 h | 0.75 | 0.11 | 0.14 | 0.81 | 0.19 |
| Measured value, 5 h | 0.73 | 0.10 | 0.17 | 0.85 | 0.15 |
| Measured value, 10 h | 0.70 | 0.11 | 0.19 | 0.85 | 0.15 |
| Measured value, 20 h | 0.69 | 0.10 | 0.21 | 0.85 | 0.15 |
| Measured value, 30 h | 0.67 | 0.14 | 0.19 | 0.79 | 0.21 |

*Bi + La + Sm = 1 and Fe + Ti = 1

Figure 4 shows the frequency dependence of thee dielectric constant and loss at room temperature for BLSFTO ceramics sintered for different time. At low frequencyy, the dielectric constant decreases sharply with the increase of frequency, while it tends to be stable at high frequency. This phenomenon is very common in dielectric materials, and this result is due to the different mechanisms of polarization at different frequencies. In general, the polarization mechanism of ferroelectric materials includes displacement polarization, turning-direction polarization and space charge polarization, and these polarization mechanisms show different relaxation time under external field. At lower frequency, all

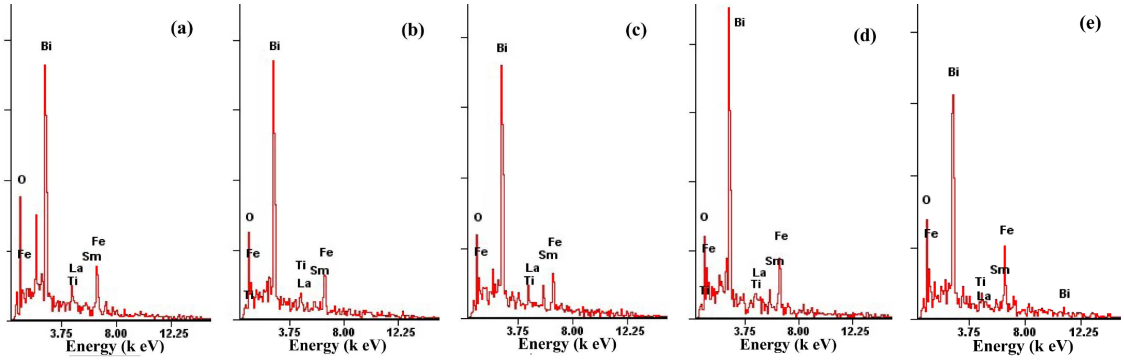


**Figure 3. EDS of BLSFTO ceramics sintered for different times: a) 2 h, b) 5 h, c)10 h, d) 20 h and e) 30 h**

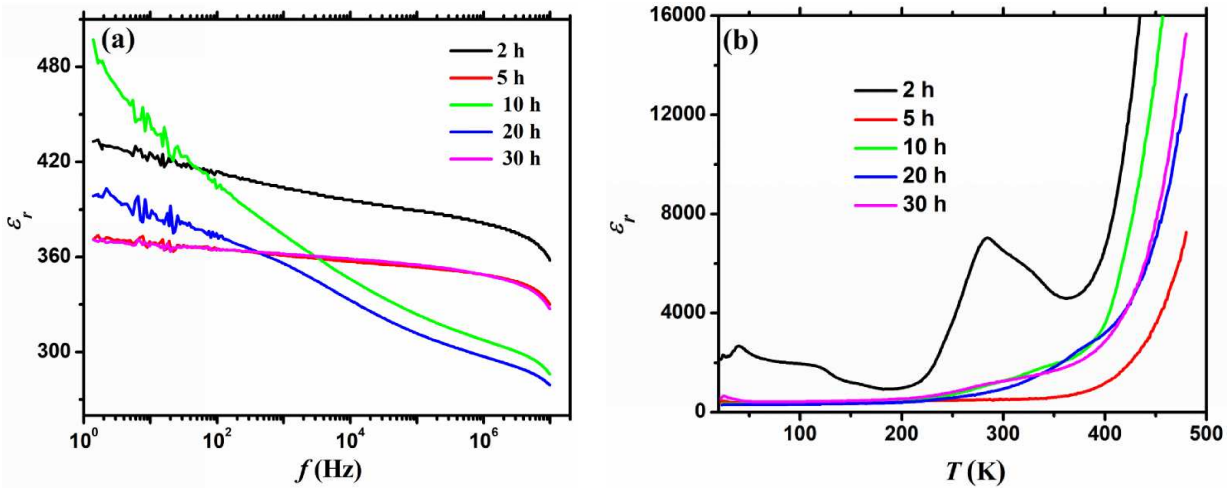


**Figure 4. Frequency dependence of the dielectric constant (a) and dielectric loss (b) of BLSFTO ceramics sintered for different times**

of the polarization processes mentioned above can be established because their relaxation time is far less than the frequency of the AC electric field. For dielectric materials, the relationship between the dielectric constant and polarization can be expressed as:

$$P = \varepsilon_0(\varepsilon_r - 1)E \tag{2}$$

where, $P$ is the polarization of the dielectric material under external electric field, $\varepsilon_0$ is the free space dielectric constant ($8.85 \times 10^{-12}$ F/m), $\varepsilon_r$ is the relative dielectric constant of the corresponding dielectric material under electric field, and $E$ is the applied external electric field. Because polarization is a function of the electric field, and it depends on the frequency of the applied field Eq. 2 can be rewritten as:

$$\varepsilon_r = 1 + \frac{1}{\varepsilon_0} \cdot \frac{\mathrm{d}p(f)}{\mathrm{d}E(f)} \tag{3}$$

It is very obvious from Eq. 3 that the relative dielectric constant is related to the frequency of the applied field because the polarization should be changed with the frequency of the measured electric field $E_m$. As a consequence, it is very clear that since electron displacement polarization, ion displacement polarization, dipole transition polarization as well as space charge polarization can be established in low frequency range, all of them can contribute to the dielectric constant and thus large constant permittivity can be obtained. However, at higher frequency, the dielectric constant is mainly contributed by the displacement polarization because the relaxation time of this polarization is in the range of $10^{-12}$–$10^{-15}$ s [32–36], which is far less than the period of the applied field (more than $10^{-6}$ s in this experiment). Other polarization mechanisms need more time to act, typical relaxation time is in the range of $10^{-3}$–$10^{-6}$ s. The different frequency stability of the dielectric constant of different samples can be attributed to the different polarization mechanisms, and the fast drop of the dielectric constant with frequency means that slow polarization process is the dominant in the material. In addition, the dielectric constant increases with the increase of the sintering time at low frequency, but this phenomenon is converse at higher frequency areas. On the whole, BLSFTO ceramics sintered for 2 h shows the largest value of the dielectric constant and the best frequency stability. The reason for this may be that although more micro-pores exist in the samples sintered for shorter time, longer sintering time can induce more impurity phases and defects, which can lead to lower dielectric constant and inferior frequency stability. It should be pointed out that the EDS results also show that the content of Bi element decreases with the sintering time and more impurities can be formed because of the decomposition of the prepared ceramics, which can be seen from the XRD patterns. The volatilization of Bi element and the impurities after the long sintering time will induce more space charges in the material, and therefore large dielectric constant can be observed in low frequency range while small values are found in high frequency. Furthermore, the sintering time can affect the grain size of BLSFTO ceramics, and the size effect can also lead to this phenomenon [37]. It should be pointed out that only the specimen sintered for 2 h shows a dielectric peak. The loss peak is provided mainly by screen charges, and the corresponding anomaly of free relaxation time appears near 290 °C. This might be because the ceramics sintered for 2 h display the smallest grain size, which can have more grain boundaries and thus the most screen charges will occurred [38,39]. The dielectric peak has never been observed in previous reports, including La, Sm and Ti doped BFO samples.

For the sake of investigating the effect of sintering time on the microstructural and multiferroic properties, room-temperature ferroelectric hysteresis loops ($P$-$E$ loops) for BLSFTO ceramics were measured at a frequency of 2 kHz, as shown in Fig. 5.

It can be seen from Fig 5 that the residual polarization intensity ($P_r$) shows non-monotonic variation with

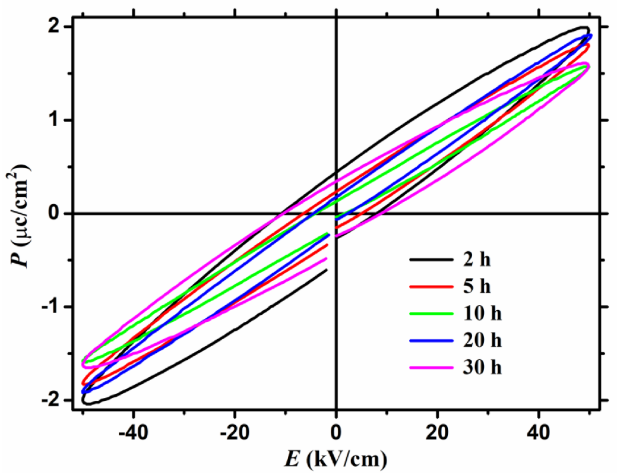


**Figure 5. Hysteresis loops of BLSFTO ceramics sintered at different time**

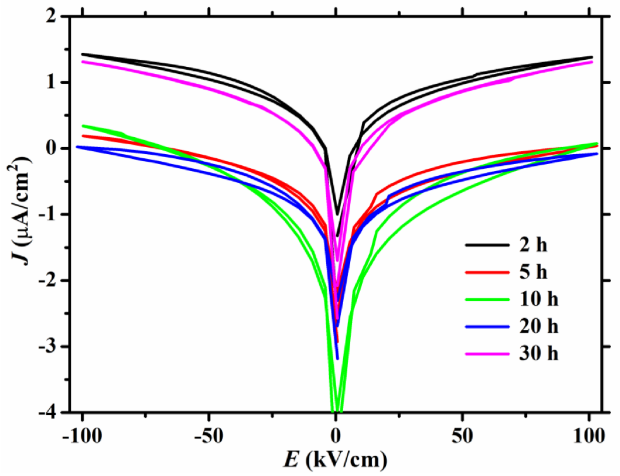


**Figure 6. *J-E* curves of BLSFTO ceramics sintered at different time**

the sintering time, i.e. it first decreases and then increases with the increase of sintering time. The maximal value can be obtained when the sintering time is 2 h. The maximum polarization intensity ($2P_r$) reaches a maximum of 1.42 μC/cm$^2$. This value is nearly the same as in other reports [35–38]. Because of the fine grains and the minimal impurities in the sample sintered for 2 h, it naturally results in preferable ferroelectric properties. However, the sample sintered for 30 h shows larger polarization compared to those sintered for 5, 10, and 20 h. The reason is that in the ceramics sintered for 30 h exists the most impurities. These impurities can generate greater leakage current, which in turn give rise to larger polarization. In addition, it can be seen from Fig. 5 that the hysteresis loop is not closed and the leakage current is large. The following reasons can explain this phenomenon. First of all, from the SEM micro-morphology, there are many pores in the ceramic sheets, which can lead to the local conductivity and thus the leakage current should be increased in the whole ceramics. Secondly, according to the XRD patterns, it can be seen that prolonged sintering time will lead to the increase of oxygen vacancy, resulting in a larger leakage current. For this reason, the leakage current of $Bi_{0.78}La_{0.08}Sm_{0.14}Fe_{0.85}Ti_{0.15}O_3$ ceramics sintered at different time was measured as a function of electric field, as shown in Fig. 6.

It can be seen from Fig. 6 that, with increasing the sintering time, the leakage current of BLSFTO ceramics gradually decreases and then increases. When the sintering time is 10 h, the leakage current is the smallest in the low field range. When the sintering times are respective 10 and 30 h, the leakage current becomes larger. The reason for the above situation may be that when the sintering time is short, such as 10 h, the samples show poor crystallization and density, whcih can induce larger leakage current. With the increase of sintering time, both the crystallization and density have been improved, less pores have been induced, therefore, the leakage current has also been reduced. However, when

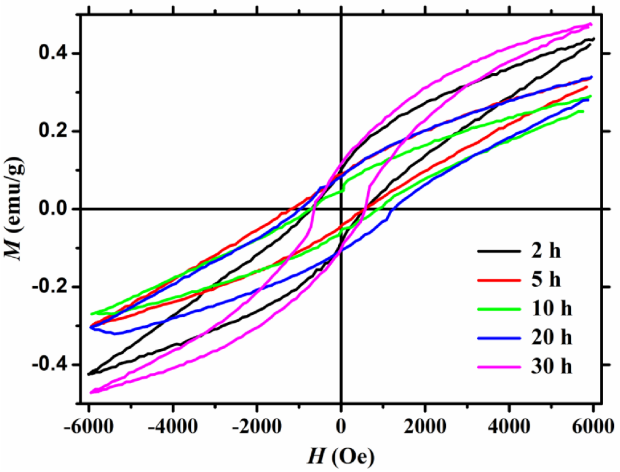


**Figure 7. *M-H* hysteresis loops of BLSFTO ceramics with different sintering time**

the sintering time is too long, for example, for 30 h, the leakage current can increase because the volatilization of Bi element increases, and the formed impurities have been increased, this impurities can result in serious leakage current.

Besides the ferroelectric properties, magnetic properties are important character of multiferroic materials. Figure 7 shows room-temperature magnetic hysteresis loops of BLSFTO ceramics annealed at different time with a maximum magnetic field of 6 kOe. The saturation magnetization increases first and then decreases with increasing the sintering time. The maximal remnant magnetization is about 0.14 emu/g when the sintering time is 2 h. This enhancement of the magnetization is larger than La and Sm doped BFO ceramics but it is consistent with the Ti doped BFO [27,28]. It is well known that, BFO is a G-type antiferromagnetic helical structure whose magnetism is derived from the atomic magnetic moment. However, its magnetic moment is not strictly anti-parallel, and there is a certain angle between adjacent magnetic moments, the helix period is 62 nm, the magnetization in one cycle strength cancel each other,

and therefore it does not show macroscopic magnetization [10–13,30–33]. Because of its special antiferromagnetic helical structure, the particle size influences the magnetic properties of BFO particularly when the size is in the nanoscale ranges [35]. Here, it can be clearly found from XRD and SEM results that the grain size monotonically increases with the increase of sintering time. Different grain size can result in different ratios of grain boundary. On one hand, the uncompensated spins will be at the grain boundary, thus the uncompensated spins increase with decreasing the grain size, which comes from the nanoscale grains in the antiferromagnetic systems and/or destroyed spiral spin structure caused by the sintering time [32–35]. On the other hand, in a crystal particle, the magnetization should be increased because of the G-type antiferromagnetic helical structure. As a result, the increased sintering time will lead to larger magnetization of the ceramics. Nonetheless, the strong magnetization for the sample sintered for 30 h may be caused by the more impurities, as shown in the XRD results. More impurities will induce more boundaries. However, the prolonged sintering time will lead to the valence change of iron ions. Furthermore, some impurities formed in the sample may show strong magnetic properties. As a consequence, the magnetization decreases firstly and then increase with increasing the sintering time on the whole.

## IV. Conclusions

In conclusion, the effect of sintering time on the structure, electrical properties and magnetic properties has been investigated systematically. All the BLSFTO ceramics sintered for different time possess pure perovskite structure except some impurities found when the sintering time is longer than 20 h. The content of Bi element decreases with the sintering time because of its volatility under high temperature, which results in the increase of impurities in the samples with longer sintering time. The average grain size and the density increase with the increase of sintering time, which results in the decrease of grain boundary and pores, while defects such as oxygen vacancies as well as some other space charges can be increased. These factors give rise to different dielectric, ferroelectric and magnetic characteristics. As a result, on the whole, the magnetism increases with the sintering time and the BLSFTO ceramics sintered for 2 h shows preferable ferroelectric properties and stability of dielectric properties. Our results provide useful information for improving multiferroic properties of BFO ceramics by combination of site engineering and sintering schedule.

**Acknowledgement:** This work has been supported by the National Natural Science Foundation of China (Grant Nos. 51372283, 51402031, 61404018, 11647036), the Chongqing Research Program of Basic Research and Frontier Technology (CSTC2018jcyjAX0416, CSTC2015jcyjA50003, CSTC2015jcyjA50015, CSTC2016jcyjA0175, CSTC2016jcyjA0349), the Young Scientific and Technological Research Program of Chongqing Municipal Education Commission (KJQN201801509), the Excellent Talent Project in University of Chongqing (Grant No. 2017-35), the Science and Technology Innovation Project of Social Undertakings and Peoples Livelihood Guarantee of Chongqing (Grant No. cstc2017shmsA0192), the Program for Innovation Teams in University of Chongqing, China (Grant No. CXTDX201601032), the Foundation of Chongqing University of Science & Technology (CK2015B05, CK2015Z13), the Latter Foundation Project of Chongqing University of Science & Technology (CKHQZZ2008002), the Scientific & Technological Achievements Foundation Project of Chongqing University of Science & Technology (CKKJCG2016328) and the Postgraduate technology innovation project of Chongqing University of Science & Technology (YKJCX1720205).

## References

1. W. Eerenstein, N.D. Mathur, J.F. Scott, "Multiferroic and magnetoelectric materials", *Nature*, **442** (2006) 759–765.
2. R.L. Gao, Z.Y. Xu, L. Bai, Q.M. Zhang, Z.H. Wang, W. Cai, G. Chen, X.L. Deng, X.L. Cao, X.D. Luo, C.L. Fu, "Electric field-induced magnetization rotation in magnetoelectric multiferroic fluids", *Adv. Electron. Mater.*, **4** [6] (2018) 1800030.
3. J. Wang, J.B. Neaton, H. Zheng, V. Nagarajan, S.B. Ogale, B. Liu, D. Viehland, V. Vaithyanathan, D.G. Schlom, U.V. WAuhmare, N.A. Spaldin, K.M. Rabe, M. Wuttig, R. Ramesh, "Epitaxial $BiFeO_3$ multiferroic thin film heterostructures", *Science*, **299** (2003) 1719–1722.
4. R.L. Gao, C.L. Fu, W. Cai, G. Chen, X.L. Deng, H.W. Yang, J.R. Sun, Y.G. Zhao, B.G. Shen, "Mechanism of ferroelectric resistive switching in $Bi_{0.9}La_{0.1}FeO_3$ thin films", *Thin Solid Films*, **583** (2015) 13–18.
5. R.L. Gao, C.L. Fu, W. Cai, G. Chen, X.L. Deng, H.R. Zhang, J.R. Sun, B.G. Shen, "Electric control of the hall effect in $Pt/Bi_{0.9}La_{0.1}FeO_3$ bilayers", *Sci. Rep.*, **6** (2016) 20330.
6. T. Choi, S. Lee, Y.J. Choi, V. Kiryukhin, S.-W. Cheong, "Switchable ferroelectric diode and photovoltaic effect in $BiFeO_3$", *Science*, **324** (2009) 63–66.
7. R.L. Gao, H.W. Yang, J.R. Sun, Y.G. Zhao, B.G. Shen, "Oxygen vacancies induced switchable and nonswitchable photovoltaic effects in $Ag/Bi_{0.9}La_{0.1}FeO_3/La_{0.7}Sr_{0.3}MnO_3$ sandwiched capacitors", *Appl. Phys. Lett.*, **104** (2014) 031906.
8. R.L. Gao, H.W. Yang, C.L. Fu, W. Cai, G. Chen, X.L. Deng, J.R. Sun, Y.G. Zhao, B.G. Shen, "Tunable photovoltaic effects induced by different cooling oxygen pressure in $Bi_{0.9}La_{0.1}FeO_3$ thin films", *J. Alloy. Compd.*, **624** (2015) 1–8.
9. K. Sardar, J.W. Hong, G. Catalan, P.K. Biswas, M.R. Lees, R.I. Walton, J.F. Scott, S.A.T. Redfern, "Structural, spectroscopic, magnetic and electrical characterization of Ca-doped polycrystalline bismuth ferrite, $Bi_{1-x}Ca_xFeO_{3-x/2}$ ($x \leq 0.1$)", *J. Phys. Condens. Matter*, **24** (2012) 045905.
10. J.J. Ruan, C. Li, Z.S. Yuan, P. Wang, A.D. Li, D. Wu,

"Four-state non-volatile memory in a multiferroic spin filter tunnel junction", *Appl. Phys. Lett.*, **109** [25] (2016) 252903.
11. R. Khomeriki, L. Chotorlishvili, I. Tralle, J. Berakdar, "Positive-negative birefringence in multiferroic layered metasurfaces", *Nano Lett.*, **16** [11] (2016). 7290–7294.
12. J.M. Hu, L.Q. Chen, C.W. Nan, "Multiferroic heterostructures integrating ferroelectric and magnetic materials", *Adv. Mater.*, **28** [1] (2016) 15–39.
13. J.J. P. Peters, G. Apachitei, R. Beanland, M. Alexe, A.M. Sanchez. "Polarization curling and flux closures in multiferroic tunnel junctions", *Nature Commun.*, **7** (2016) 13484.
14. H. Palneedi, V. Annapureddy, S. Priya, J. Ryu, "Status and perspectives of multiferroic magnetoelectric composite materials and applications", *Actuators*, **5** [1] (2016) 9–39.
15. T. Hussain, S.A. Siddiqi, S. Atiq, M.S. Awan, "Induced modifications in the properties of Sr doped $BiFeO_3$ multiferroics", *Prog. Natur. Sci. Mater. Intern.*, **23** (2013) 487–492.
16. E. Ruff, S. Krohns, M. Lilienblum, D. Meier, M. Fiebig, P. Lunkenheimer, A. Loidl, "Conductivity contrast and tunneling charge transport in the vortexlike ferroelectric domain patterns of multiferroic hexagonal $YMnO_3$", *Phys. Rev. Lett.*, **118** [3] (2017) 036803.
17. Y. Wei, C. Jin, Y. Zeng, X. Wang, D. Gao, X. Wang. "A coexistence of multi-relaxor states in $0.5BiFeO_3$-$0.5BaTiO_3$", *Ceram. Int.*, **43** [18] (2017) 17220–17224.
18. C.A.F. Vaz, "Electric field control of magnetism in multiferroic heterostructures", *J. Phys. Condens. Matter*, **24** [33] (2012) 333201.
19. A. Agbelele, D. Sando, C. Toulouse, C. Paillard, R.D. Johnson, R. Ruffer, A.F. Popkov, C. Carretero, P. Rovillain, J.M.L. Le Breton, B. Dkhil, M. Cazayous, Y. Gallais, M.A. Measson, A. Sacuto, P. Manuel, A.K. Zvezdin, A. Barthelemy, J. Juraszek, M. Bibes, "Strain and magnetic field induced spin-structure transitions in multiferroic $BiFeO_3$", *Adv. Mater.*, **29** (2017) 1602327.
20. S. Dong, J.M. Liu, S.W. Cheong, Z.F. Ren, "Multiferroic materials and magnetoelectric physics: Symmetry, entanglement, excitation, and topology", *Adv. Phys.*, **64** [5] (2015) 519–626.
21. J.H. Lee, C. Yoon, S. Lee, Y.H. Kim, B.H. Park, "Direct observation of domain motion synchronized with resistive switching in multiferroic thin films", *ACS Appl. Mater. Interface*, **8** [51] (2016) 35464–35471.
22. J.M. Zhang, Y. Huang, L. Jin, F. Rosei, F. Vetrone, J.P. Claverie, "Efficient upconverting multiferroic core@shell photocatalysts: visible-to-near-infrared photon harvesting", *ACS Appl. Mater. Interf.*, **9** [9] (2017) 8142–8150.
23. W. Ge, A. Rahman, H. Cheng, M. Zhang, J. Liu, Z. Zhang, B. Ye, "Probing the role of cation vacancies on the ferromagnetism of La-doped $BiFeO_3$ ceramics", *J. Magn. Magn. Mater.*, **449** (2018) 401–405.
24. D.P. Dutta, A.K. Tyagi, "Effect of $Sm^{3+}$ and $Zr^{4+}$ codoping on the magnetic, ferroelectric and magnetodielectric properties of sonochemically synthesized $BiFeO_3$ nanorods", *Appl. Surface Sci.*, **450** (2018) 429–440.
25. T. Durga Rao, K.R. Kandula, A. Kumar, S. Asthana, "Improved magnetization and reduced leakage current in Sm and Sc co-substituted $BiFeO_3$", *J. Appl. Phys.*, **123** [24] (2018) 244104.
26. A. Panda, R. Govindaraj, K. Vinod, P. Magudapathy, G. Amarendra, "Magnetic and structural studies in pristine and La doped $BiFeO_3$ using Mössbauer spectroscopy", *AIP Conf. Proceed.*, **1951** (2018) 030020.
27. J.-H. Zhu, J.-Q. Dai, J.-W. Xu, X.-Y. Li, "Effect of Zn and Ti co-doping on structure and electrical properties of $BiFeO_3$ ceramics", *Ceram. Int.*, **44** [8] (2018) 9215–9220.
28. N. Kumar, A. Shukla, "Processing and characterization of Cd/Ti co-substituted $BiFeO_3$ nanoceramics", *Int. J. Modern Phys. B.*, **32** [19] (2018) 1840069.
29. B.S. Soram, B.S. Ngangom, H.B. Sharma, "Effect of annealing temperatures on the structural and optical properties of sol-gel processed nanocrystalline $BiFeO_3$ thin films", *Thin Solid Films*, **524** (2012) 57–61.
30. A. Chaudhuri, K. Mandal, "Large magnetoelectric properties in $CoFe_2O_4$:$BaTiO_3$ core-shell nanocomposites", *J. Magn. Magn. Mater.*, **377** (2015) 441–445.
31. T. Kawae, Y. Terauchi, H. Tsuda, M. Kumeda, A. Morimoto. "Improved leakage and ferroelectric properties of Mn and Ti codoped thin films", *Appl. Phys. Lett.*, **94** (2009) 112904.
32. R.Z. Xiao, V.O. Pelenovich, D.J. Fu, "Spin cycloid destruction in Pr doped $BiFeO_3$ films studied by conversion-electron Mossbauer spectroscopy", *Appl. Phys. Lett.*, **103** (2013) 012901.
33. T.X. Li, H.W. Wang, Z. Hu, K.S. Li, "Temperature dependence of magnetoelectric coupling in $La_{0.7}Sr_{0.3}MnO_3/BaTiO_3$ layered heterostructure with various volume fraction", *Thin Solid Films*, **616** (2016) 1–5.
34. A.S. Kumar, C.S.C. Lekha, S. Vivek, V. Saravanan, K. Nandakumar, S.S. Nair, "Multiferroic and magnetoelectric properties of $Ba_{0.85}Ca_{0.15}Zr_{0.1}Ti_{0.9}O_3$-$CoFe_2O_4$ core-shell nanocomposite", *J. Magn. Magn. Mater.*, **418** (2016) 294–299.
35. F. Yan, T.J. Zhu, M.O. Lai, L. Lua, "Enhanced multiferroic properties and domain structure of La-doped $BiFeO_3$ thin films", *Scripta Mater.*, **63** (2010) 780–783.
36. J.A. Schiemer, R.L. Withers, Y. Liu, M.A. Carpenter, "Ca-doping of $BiFeO_3$: The role of strain in determining coupling between ferroelectric displacements, magnetic moments, octahedral tilting, and oxygen-vacancy", *Chem. Mater.*, **25** (2013) 4436–4446.
37. X.W. Tang, J.M. Dai, X.B. Zhu, Y.P. Sun, "In situ magnetic annealing effects on multiferroic Mn-doped $BiFeO_3$ thin films", *J. Alloys Compd.*, **552** (2013) 186–189.
38. P. Uniyal, K.L. Yadav, "Pr doped bismuth ferrite ceramics with enhanced multiferroic properties", *J. Phys. Condens. Matter*, **21** (2009) 405901.
39. V. Verma, A. Beniwal, A. Ohlan, R. Tripathi. "Structural, magnetic and ferroelectric properties of Pr doped multiferroics bismuth ferrites", *J. Magn. Magn. Mater.*, **394** (2015) 385–390.